A CubeSat mission dedicated to monitor lunar horizon glow

Orger Necmi Cihan, Cordova Alarcon Jose Rodrigo, Minh Pham Anh, Kim Sangkyun, Kitamura Kentaro, Teramoto Mariko, Nakayama Daisuke, Kishimoto Makiko, Nishinaga Kounosuke, Oboshi Akihiro, Sawa Kenta, Masui Hirokazu, Sano Kei, Toyoda Kazuhiro, Cho Mengu (Kyushu Institute of Technology)

Abstract

Lunar horizon glow (LHG) has been seen as an excessive brightness to be monitored in order to estimate the abundance of the exospheric dust grains near the lunar terminator. Monitoring the LHG could reveal critical information on the dust particles near surface and at low altitudes that is extremely critical for the safety of human and robotic explorers. In this study, a CubeSat mission called Horyu-VI is proposed with a multispectral camera as a payload to detect the light scattering above the lunar horizon. It is planned as a 6U CubeSat mission with a 100 km circular orbit, and the secondary mission is considered as monitoring the space weather. During the main mission, the light-scattering events are planned to be captured with multispectral images in various wavelengths such as UV, visible and NIR. As a result, the observations will help to improve our understanding of dust population near the lunar terminator.

1. Introduction

Lunar dust is the smallest component of the lunar regolith that is produced by impact events and space weathering. Even though it was anticipated before the Apollo-era missions (Jaffe, 1965), the environmental effect of the lunar dust must be nonetheless highlighted for the future manned and robotic missions. The lunar dust grains, which are significantly sharper than any simulant particles on Earth, cause several problems for manned (Harris, 1972; Gaier and Creel, 2005; James et al., 2009; Linnarsson et al., 2012) and robotic missions (Gaier and Creel, 2005; Gaier and Jaworske, 2007; O'Brien, 2011, 2018) such as in Table 1.

Table 1. The problems and risk factors for manned and unmanned missions due to lunar dust.

The problems for unmanned missions
• Decreasing solar panel efficiency
• Invalid sensor readings
• Instrument malfunctions
• Altered optical observations
• Spacecraft material degradation
• Thermal property alterations
• Discharges on critical components
• Obstruction of moving mechanisms
• Sealing failures
The risk factors for astronauts on the lunar surface
• Irritation and breathing problems
• Developing fever after breathing the dust
• Contamination of habitats and astronaut suits
• Problems with eyesight
• Future health problems due to long-term exposure

It is important to understand that improving our knowledge about the dust environment near the lunar surface can advance many aspects of planetary surface science and exploration by humans and robotic missions (Szalay et al., 2018). Since the Apollo-era observations, the LHG has been seen as an excessive brightness above the lunar horizon to be monitored by the orbiters and landers watching sunrise or sunset to estimate the abundance of the exospheric dust grains near the terminator (Criswell, 1973; McCoy and Criswell, 1974; McCoy, 1976; Rennilson and Criswell, 1974; Severnyi et al., 1975; Zook and McCoy, 1991; Colwell et al., 2007; Glenar et al., 2011; Glenar et al., 2014; Feldman et al., 2014; Barker et al.; 2019).
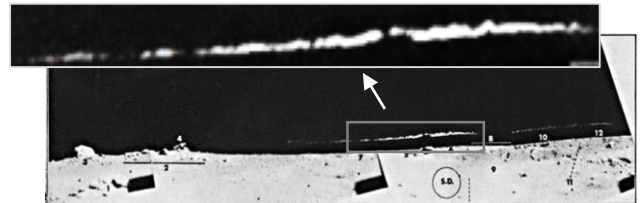

Figure 1. The lunar horizon glow photograph by Surveyor 7 (Criswell, 1973)

The LHG could reveal significant information on the dust population near surface and at low altitudes that is extremely important for the safety of human and robotic explorers (Fig. 1). There has been no dedicated mission to observe the LHG simultaneously in multiple wavelengths,

and a small satellite platform can continuously monitor the light scattering above the lunar terminator region to detect the column density of the lunar dust cloud.

In this paper, A CubeSat mission dedicated to monitor the LHG called Horyu-VI is explained. Observation method and requirements are defined in section 2. Satellite configuration is described in section 3. Finally, the conclusion and discussion are given in section 4.

2.   Observation Method and Requirements

The lunar dust population is known to be asymmetrical between sunrise and sunset terminator according to the LEAM sensors (Berg et al. 1976), and the overall dust exosphere is reported to be asymmetrical related to the direction of the meteoroid streams producing tenuous dust cloud around the Moon (Horanyi et al., 2015; Szalay et al., 2018). Therefore, observing both terminators for the light scattering in the same orbit is advantageous to make a comparison.
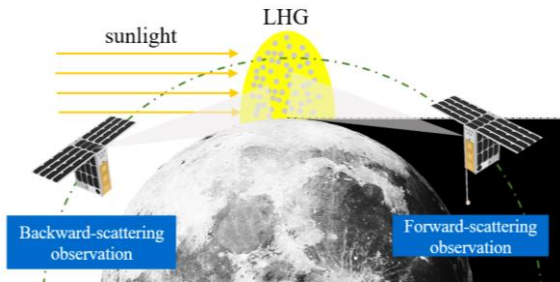

Figure 2: Forward and backward light scattering observations
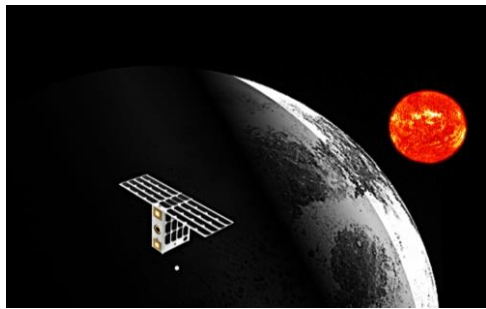

Figure 3. Horyu-VI during orbital sunrise

According to Mie light scattering theory, the forward-scattering of the sunlight will be more intense than the backward-scattering (Fig. 2). In addition, previous observations pointed out that sunrise driven dust population be denser than the dust cloud on the sunset region. Therefore, it is expected to capture the brightest horizon images from the shadow cylinder of the Moon on the sunrise terminator (Fig. 3).

Mie scattering theory can be used to detect particle abundance with the sizes in the range of $\lambda/10 - \lambda$, which means the scattered light wavelength is comparable to the dust particle diameter. Therefore, multispectral camera payload must be configured accordingly. As it is seen in Fig. 4, coronal and zodiacal light (CZL), which is the light scattering by the interplanetary dust particles, can easily saturate the captured images. As a result, low-altitude orbits are useful to block a large part of the CZL by the lunar surface.

In addition to the forward and backward light-scattering observations, there are two approaches to study the LHG on orbit:

- Monitoring entire light scattering of dust column estimated by Apollo sketches up to the upper limit of the dust exosphere, which is approximately from 100 to 200 km (Glenar et al., 2011).
- Monitoring decreasing brightness with altitude by focusing on horizon rim, which requires <100 m/pixel resolution.
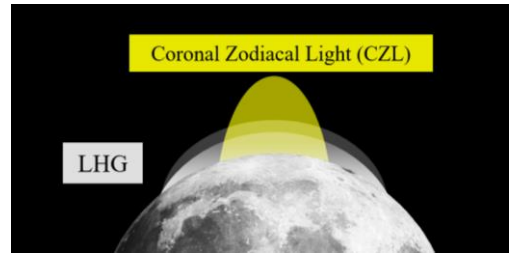

Figure 4: LHG overlapping with CZL

Since the lunar dust population is expected to be from sub-micron to micrometer range, the wavelength bands for the multispectral camera payload is given in Fig. 5.
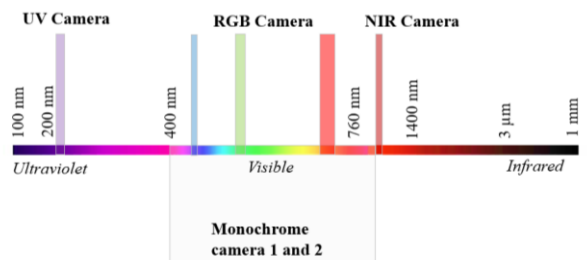

Figure 5: Wavelength coverage for the observation with multispectral camera payload

First, the brightness variation by altitude is planned to be detected per 100 m over the lunar terminator. Since it requires <100 m/pixel resolution, the image frame will see a narrow area over the horizon. In addition, the high-

altitude LHG observations by Apollo point out that the responsible dust cloud was extending in the range of 10s of km above the lunar terminator (Glenar et al., 2011). However, there is a high uncertainty due to astronaut drawings. Therefore, the captured image is expected to be covering up to 50 km from the center of the image frame while the ADCS pointing the cameras on the horizon line. The dust population is expected to be smaller than 1 micrometer in diameter. As a result, the wavelength targets are selected as visible, near-infrared and RGB bands.

Table 3. Payload requirements for observation.

Observation	Requirement
Narrow Coverage	1. Detecting brightness variation per 100m altitude 2. Monitoring brightness at VIS/NIR/RGB wavelengths up to 50 km altitude from the center of the image
Wide Coverage	Monitoring overall brightness at visible and UV wavelengths up to 200 km altitude from the center of image
Overall Image sequence	Capturing sequence of images around orbital sunrise and sunset positions (3-4 minutes duration)

Table 4. Multispectral camera configuration.

Configuration	Band / Channel	CWL (nm)	FWHM (nm)	Focal Length (mm)
Monochrome camera 1	VIS	-	-	25
Monochrome camera 2		-	-	8
RGB Camera	R	464	23	20
	G	542	27	
	B	639	42	
Near-Infrared Camera	NIR	850	10	
UV Camera	UV	250	10	8

The exospheric dust cloud is expected to collapse below 100-200 km altitude, and it covers the most tenuous part of the dust population, which is submicron to nanometer range. Therefore, the captured image is expected to be covering up to 200 km from the center of the image frame while the ADCS pointing the cameras on the horizon line, and the wavelength targets are selected as visible and ultra-violet bands. Finally, the ADCS should be able to point the cameras on the horizon line since wider angles will decrease the brightness observed by the camera sensor. These requirements are summarized in Table 3 and 4.

3. Horyu-VI Overview

Horyu-6 configuration is based on 6U CubeSat standard that is 100 mm x 226.3 mm x 340.5 mm (Fig. 6). After the deployment of the solar panels and the magnetometer, the dimensions will become 740.0 mm x 226.3 mm x 643.0 mm. Horyu-VI overview is described in Table 5.
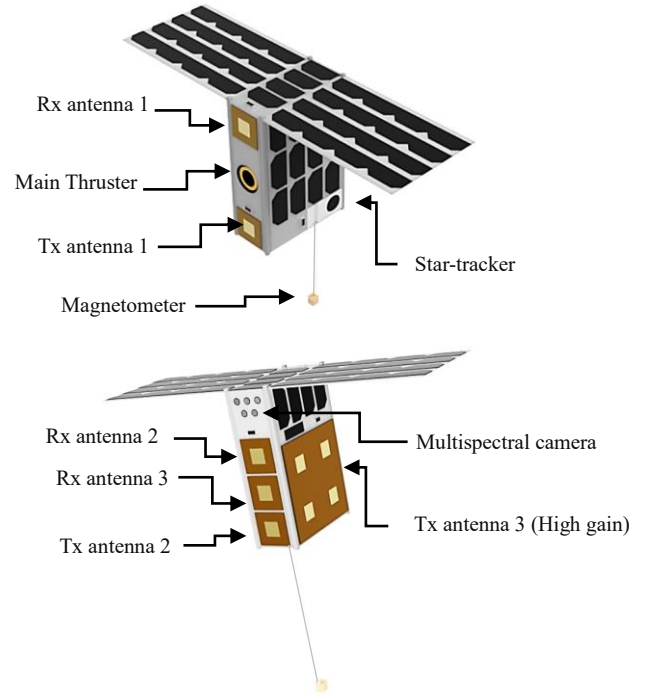

Figure 6. Horyu-VI drawing.

Table 5. Horyu-VI Configuration

Dimensions (mm)	Stowed: 100.0 x 226.3 x 340.5 Deployed: 740.0 x 226.3 x 643.0
Mass (kg)	10.2
Planned mission lifetime	1 year
On-board data handling	Kyutech OBC with 1-Gbit storage, UART and SPI interfaces, Watchdog timer for Reset PIC
EPS	Generation: 32 solar cells on deployable panels, 24 solar cells on body mounted panels Storage: 74.5 Wh battery capacity, battery temperature control
AOCS	ADCS: 3 x Reaction wheels, star tracker, gyroscope, 6 x sun sensors, control board, adapter board Propulsion: Integrated hall effect thruster + 4 x resistojets
Satellite tracking	OPERA mission with CSAC 1 x S-band Rx antenna
Communication	S-band uplink: 1bps – 16bps S-band downlink: 30bps – 3kbps S-band CW beacon 1 x High-gain Tx antenna 2 x Low-gain Tx antenna 2 x Low-gain Rx antenna

Payload	Multispectral camera payload Space weather magnetometer Spacecraft surface potential probe

3.1. AOCS

The AOCS subsystem consists of (1) integrated ADCS unit, (2) main propulsion system, (3) Secondary thrust system, and (4) external sun sensors. Fig. 7 shows a simplified diagram of the AOCS interfaces, where the AOCS interface/control board serves as an interface between the AOCS hardware and the OBC. The AOCS interface/control board will perform the following tasks:

- Send commands to the AOCS hardware and save the telemetry data
- Control the power supply of the AOCS hardware
- Calculate the target attitude during Earth tracking, science mode, and orbit correction maneuvers
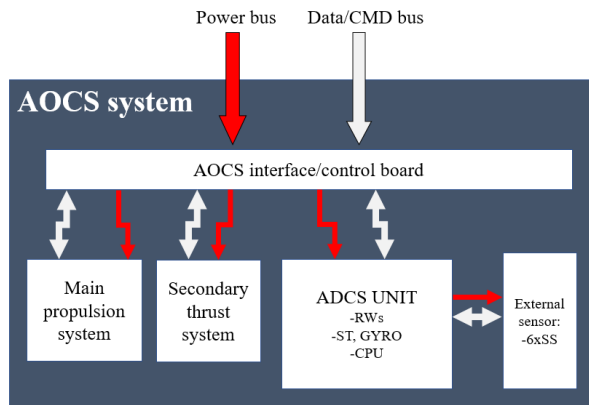

Figure 7. AOCS overview and configuration.

Table 6. AOCS modes of operation.

Modes	AOCS Requirement
De-tumbling	Rough angular rate estimation (<1deg error) Gyroscope Reaction wheels
Sun tracking	Determination of the Sun direction (<5deg error) Sun sensors or star tracker Reaction wheels
Earth tracking	Estimation of the Earth direction Star tracker (<5deg error) Reaction wheels
Science	Estimation of the lunar horizon direction Star tracker (<0.1deg error) Reaction wheels (slew rate < 1deg/s)
Orbit correction maneuvers	Estimation of the thrust direction Star tracker (<0.1deg error) Reaction wheels Main thruster (<200uN thrust)
Reaction wheels desaturation	Spin rate of reaction wheels Secondary thrusters (<10uNm torque)

The AOCS modes of operation are listed in Table 6. It includes the pointing requirement and the actuators required for each mode of operation.

In science mode, the lunar horizon pointing modes are categorized into three strategies, forward-pointing, backward-pointing, and forward-backward pointing (Fig. 8). Whereas single forward and backward-pointing requires less attitude maneuvering (slew rates < 0.05deg/s), the forward-backward pointing strategy requires 2 large-angle maneuvers per orbit; however, the reaction wheels will not be saturated by these periodic maneuvers since the subsequent maneuver is performed in the opposite direction.
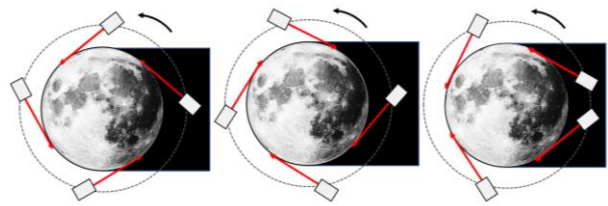

Figure 8. The methods of forward pointing (left), backward pointing (middle), and forward-backward ¥pointing (right)

The propulsion system includes one main thruster (<200uN of thrust) and 4 secondary thrusters (<50uN per thruster) whose alignment can be customized. The overall size of the propulsion system is 100mm x100mm x 200mm, which includes the propellant tank, thruster heads, and a control board. The amount of ΔV that can provide this propulsion system is 120m/s and the estimated torque induced by the secondary thrusters is <10uNm. The initial proposed design considers the use of the main thruster capable of orbit correction maneuvers and 4 secondary thrusters for the desaturation of reaction wheels. The small thrusters are placed in pyramidal configuration to induce a controlled torque in the 3 axes of the spacecraft (Speretta et al., 2019).

3.2. Communication and Satellite Tracking

Horyu-VI uses S-band frequencies for uplink and downlink. S-band communication subsystem is connected to a high-gain Tx antenna, 2 low-gain Tx antennas, and 2 low-gain Rx antennas. The uplink speed is 1bps – 16bps, and the downlink speed is estimated to be 30bps – 3kbps.

S-band board consumes 3W in Rx mode, whereas it consumes 6W during nominal speed transmission and 20W during high-speed transmission.

Satellite tracking is performed over OPERA subsystem, which consists of a software-defined radio, a processing board, chip-scale atomic clock (CSAC) and a patch antenna. Accuracy requirement is determined to be 5 km, and the resolution requirement is calculated as 1/10 of the accuracy requirement. In addition, the subsystem power consumption is approximately 4.5W, and the signal modulation is SS-BPSK.

3.3. Secondary Payloads

As the secondary mission, an observation of the IMF (Interplanetary Magnetic Field), which is frozen-in to the solar wind plasma and is expanded from the surface of the sun, is proposed. The magnetic field observation system is named MGF (MaGnetic Field measurement system), which will be developed based on the established technology of Fluxgate (FG) magnetometer. The observation of the IMF has been conducted by several spacecraft as a fundamental parameter to diagnose the condition of solar wind. However, a demonstration of the IMF observation by the miniaturized FG magnetometer can be significant turning point to promote the observation of the interplanetary space by the CubeSats.

The main scientific objectives of the secondary mission are defined in following three topics:

1. Observation of the IMF structure
2. Observation of the Aflvén Wave in the high-speed solar wind
3. Observation of the ULF wave in lunar wake region

To achieve above three observations, the magnetometer for the Horyu-VI is required as described below:

1. Intensity of IMF < 10nT
   - Requirement of resolution is < 0.1nT
2. For ULF (Ultra-Low Frequency) wave:
   - Period: $0.001 - 1$ s
   - Amplitude is $\sim 0.1 - 5$nT
   - Requirement of resolution is < 0.01nT
3. Deployment of the magnetometer

The basic performance of the magnetometer is typical as a FG magnetometer onboard the conventional satellites for solar wind observation. However, miniaturization of the FG magnetometer, which makes it possible to observe the small perturbation of IMF by the CubeSats, is quite important and breakthrough challenge for the future deep space mission by the CubeSats.

Another secondary payload is proposed as spacecraft surface charging probe. Both magnetometer and surface charging probe will be indicator for the space weather conditions during the LHG observations.

4. Conclusions

In this paper, a lunar CubeSat mission dedicated for observing the light-scattering events over the lunar terminator region is described. The satellite is proposed to be a 6U CubeSat with a capability to monitor the lunar horizon during orbital sunrise and sunset passages while capturing image sequences. In addition, the secondary payloads will be able to monitor the space environment conditions during these observations. Therefore, the objectives can be summarized as monitoring the brightness of the lunar horizon, using the brightness data to retrieve the dust column density above the lunar terminator, collect data of the magnetic field and spacecraft surface potential, and demonstrate the satellite tracking by OPERA subsystem as a lunar CubeSat mission.

References

1) Jaffe, L.D., 1965. Depth of the lunar dust. Journal of Geophysical Research70, 6129–6138.
2) Harris, R.S., 1972. Apollo experience report: Thermal design of Apollo lunar surface experiments package. National Aeronautics and Space Administration.
3) Horanyi, M., Szalay, J., Kempf, S., Schmidt, J., Grün, E., Srama, R., Sternovsky, Z., 2015. A permanent, asymmetric dust cloud around the moon. Nature 522, 324–326.19
4) Gaier, J.R., Creel, R.A., 2005. The effects of lunar dust on eva systems during the Apollo missions.
5) Gaier, J.R., Jaworske, D.A., 2007. Lunar dust on heat rejection system surfaces: problems and prospects, in: AIP Conference Proceedings, American Institute of Physics. pp. 27–34.
6) James, J.T., Lam, C.w., Quan, C., Wallace, W.T., Taylor, L., 2009. Pul-monary Toxicity of Lunar Highland Dust. Technical Report. SAE Technical Paper.
7) Linnarsson, D., Carpenter, J., Fubini, B., Gerde, P., Karlsson, L.L., Loftus, D.J., Prisk, G.K., Staufer, U., Tranfield, E.M., van Westrenen, W., 2012. Toxicity of lunar dust. Planetary and Space Science 74, 57–71.
8) O'Brien, B.J., 2011. Review of measurements of dust movements on the

Moon during Apollo. Planetary and Space Science 59, 1708–1726.

9) O'Brien, B.J., 2018. Paradigm shifts about dust on the moon: From Apollo 11 to Chang'e-4. Planetary and Space Science 156, 47–56.

10) Szalay, J. R., Poppe, A. R., Agarwal, J., Britt, D., Belskaya, I., Horányi, M., Nakamura, T., Sachse, M. and Spahn, F., 2018. Dust phenomena relating to airless bodies. Space Science Reviews, 214(5), 98.

11) Criswell, D.R., 1973. Horizon-glow and the motion of lunar dust, in: Photonand Particle Interactions with Surfaces in Space. Springer, pp. 545–556.

12) McCoy, J. E., Criswell, D. R., 1974. Evidence for a high altitude distribution of lunar dust. In *Lunar and planetary science conference proceedings*, 5, pp. 2991-3005.

13) McCoy, J.E., 1976. Photometric studies of light scattering above the lunar terminator from apollo solar corona photography, in: Lunar and PlanetaryScience Conference Proceedings, pp. 1087–1112.

14) Rennilson, J.J., Criswell, D.R., 1974. Surveyor observations of lunar horizon-glow. The Moon 10, 121–142.

15) Severny, A., Terez, E., Zvereva, A., 1975. The measurements of sky brightnesson lunokhod-2. The Moon 14, 123–128.

16) Zook, H. A., McCoy, J. E., 1991. Large scale lunar horizon glow and a high altitude lunar dust exosphere. Geophysical Research Letters, 18(11), 2117-2120.

17) Colwell, J.E., Batiste, S., Horanyi, M., Robertson, S., Sture, S., 2007. Lunar surface: Dust dynamics and regolith mechanics. Reviews of Geophysics 45, RG2006.

18) Glenar, D.A., Stubbs, T.J., McCoy, J.E., Vondrak, R.R., 2011. A reanalysis of the Apollo light scattering observations, and implications for lunar exospheric dust. Planetary and Space Science 59, 1695–1707.

19) Glenar, D.A., Stubbs, T.J., Hahn, J.M., Wang, Y., 2014. Search for a high-altitude lunar dust exosphere using Clementine navigational star tracker measurements. Journal of Geophysical Research: Planets 119, 2548–2567.

20) Feldman, P.D., Glenar, D.A., Stubbs, T.J., Retherford, K.D., Gladstone,G.R., Miles, P.F., Greathouse, T.K., Kaufmann, D.E., Parker, J.W., Stern,S.A., 2014. Upper limits for a lunar dust exosphere from far-ultraviolet spectroscopy by LRO/LAMP. Icarus 233, 106–113.

21) Barker, M., Mazarico, E., McClanahan, T., Sun, X., Neumann, G., Smith, D., Zuber, M., Head, J., 2019. Searching for lunar horizon glow with the lunar orbiter laser altimeter. Journal of Geophysical Research: Planets 124, 2728–2744.

22) Berg, O.E., Wolf, H., Rhee, J., 1976. Lunar soil movement registered by the Apollo 17 cosmic dust experiment. Interplanetary dust and zodiacal light. Springer, pp. 233–237.

23) Speretta, S., Cervone, A., Sundaramoorthy, P., Noomen, R., Mestry, S., Cipriano, A., Topputo, F., Biggs, J., Di Lizia, P., Massari, M. and Mani, K.V., 2019. LUMIO: an autonomous CubeSat for lunar exploration. In *Space operations: inspiring Humankind's future* (pp. 103-134). Springer, Cham.